Advances in Nanoparticles, 2017, 6, 11-21
http://www.scirp.org/journal/anp
ISSN Online: 2169-0529
ISSN Print: 2169-0510

A Facile Synthesis and Photoluminescence Properties of SiO_2:Tb^{3+} Spherical Nanoparticles

Murad M. A. Abualrejal, Haifeng Zou*, Jie Chen, Yanhua Song, Ye Sheng*

College of Chemistry, Jilin University, Changchun, China
Email: 1726389572@qq.com

How to cite this paper: Abualrejal, M.M. A., Zou, H.F., Chen, J., Song, Y.H. and Sheng, Y. (2017) A Facile Synthesis and Photoluminescence Properties of SiO_2:Tb^{3+} Spherical Nanoparticles. *Advances in Nanoparticles*, **6**, 11-21.
https://doi.org/10.4236/anp.2017.62002

Received: February 24, 2017
Accepted: March 18, 2017
Published: March 21, 2017

Abstract

Controlled synthesis of functional photoluminescent materials are of particular interest due to their fascinating optical properties. Herein, highly uniform SiO_2:xTb^{3+}spherical nanoparticles are fabricated by a facile sol-gel method. The structure, morphology, compositions, and luminescence properties of As-prepared samples were well investigated using TEM, SEM, EDX, XRD, XPS and luminescence spectroscopy. The PL intensity of SiO_2:xTb^{3+}spherical nanoparticles is Tb^{3+} ions concentration dependent achieved a maximum at 3 mol % of Tb^{3+}. Particularly, SiO_2:xTb^{3+}spherical nanoparticles exhibit a green emission corresponding to $^5D_4 \rightarrow {}^7F_j$ transition (541 nm) of Tb^{3+}. These results show that As-prepared phosphors may find potential application in solid-state lighting fields.

Keywords

Silica, Sol-Gel, Photoluminescence, Terbium Doped-Silica

1. Introduction

Lanthanides have unique photoluminescence properties, which enables their utilization in diverse applications, such as optical devices [1], biological fluorescence imaging and detections [2] [3] [4] [5] [6], lighting and displays [7] [8] [9] depending on their morphology, size, and composition [10]. Particularly, Tb^{3+} is an intriguing trivalent lanthanides ion due to its green light emission under near-ultraviolet excitation. Silica is a fantastic oxide bolster material for an extensive variety of applications, such as electronics, displays, sensors, catalysts, and biomedical imaging, due to its thermal stability and endurable biocompatibility [11]-[17]. In addition, the silica spine cannot only serve to bulwark and firm the functional structure inside but also allow its optical properties to be inquired from outside due to the chemical activity and optical transparency of si-

lica [18]. Furthermore, numerous researchers have been dedicated to the synthesis of rare earth ions doped SiO_2 materials with different morphologies via various synthesis methods. For example, Chen Jie *et al.* have successfully prepared SiO_2:Eu^{3+} fibers by both electrospinning technique and sol-gel process [19]. Gao Fei *et al.* prepared europium (III)-doped silica nanotubes by sol-gel method and discussed many influencing factors such as NH_4OH addition, stirring time and the formation mechanism [20]. Lidia Armelao *et al.* have reported the formation of strong O-Tb complex resulting in reducing the high frequency oscillators and enhancing the PL intensity [10]. The oxidation state of Tb(III) ions is very stable in a silica matrix, hence strong green luminescence can be obtained by a high temperature thermal-annealing treatment having reported by Choi *et al.* [21]. Inspired by this, herein we have synthesized SiO_2:xTb^{3+} nanospheres by sol-gel method in this work, which is facilitating homogeneous doping of Tb^{3+} into SiO_2 matrix without segregation that is highly required to increase the PL activity. The structure, morphology, and photoluminescence properties of SiO_2:xTb^{3+} nanospheres were investigated as a function of Tb^{3+} concentration.

2. Experimental Section

2.1. Materials

Cetyltrimethylammonium bromide (CTAB), Ammonia, ethanol, were purchased from Beijing Chemical. Tetraethyl orthosilicate (TEOS) was bought from Aladdin Reagent Database Inc. All chemicals were of analytical grade and were used directly without further purification. $Ln(NO_3)_3$ was prepared by dissolving the corresponding Sm_2O_3 (99.99%) and Tb_4O_7 (99.99%) powder in dilute HNO_3 solution at elevated temperature with ceaseless agitation.

2.2. Preparation

A series of rare earth-doped SiO_2 spherical nanoparticles were prepared via a simple CTAB-based sol-gel process. In a typical process, 0.35 g CTAB was dissolved in 5 mL ethanol and 20 ml deionized water. After stirring several minutes, 0.3 ml Ammonia, 2.2 ml TEOS and different amount of $Ln(NO_3)_3$ were added into the above solution, respectively. After additional agitation for overnight, the resulting precipitates were collected by centrifugation, washed three times with ethanol, deionized water, and then dried at 60˚C in air for 12 h. The final product was obtained through a heat treatment of the precursor at 600˚C in air for 2 h.

2.3. Characterizations.

X-ray powder diffraction (XRD) was measured by a Rigaku D/max-B II X-ray diffractometer with Cu Ka radiation. Transmission electron microscopy (TEM) images were obtained with a JEM-2000EX TEM (acceleration voltage of 200 kV). The scanning electron microscope (SEM) images were observed by S-4800, Hitachi. Energy-dispersive spectroscopy (EDS) analysis was performed with an H JEOL JXA 840 EDX system attached to the SEM microscope. The X-ray photoe-

lectron spectra (XPS) were taken using a VG ESCALAB 250 electron energy spectrometer with Mg Ka (1253.6 eV) as the X-ray excitation source. The PL measurements were determined using Jobin Yvon FluoroMax-4 luminescence spectrophotometer (PL) equipped with a 150 W xenon lamp as the excitation source. All the measurements were performed at room temperature.

3. Results and Discussion

3.1. Morphologies and Structures

The morphologies and structures of samples were investigated by the SEM and TEM observations. (Figure 1(a)) shows the SEM image of the as-prepared SiO_2:Tb^{3+} spherical nanoparticles as we can see, the morphologies of these SNPs are uniform with a high purity approaching 100%. The decomposition of the organic components (such as CTAB) was further verified by the typical high-magnification transmission electron microscopy (TEM) images as shown in (Figure 1(b)). SiO_2:Tb^{3+}nanoparticles are highly dispersed with a narrow size distribution (Figure 1(c)). The average diameter of products was 102.5 ± 4.2 nm and several tens to hundreds of nanometers in length, which were determined by manually measuring 50 randomly selected sphere (Figure 1(d)) by ImageJ. Interestingly, HR-TEM images reveal that these nanoparticles are spherical-like without any undesired impurities observed (Figure 1(e)). Moreover, the selected area electron diffraction (SAED) pattern (Figure 1(f)) shows that the silica doped Tb^{3+} ion is amorphous and no facilities which in agreement with the XRD pattern.

The structure and composition of the as-prepared SiO_2:Tb^{3+} spherical nanoparticles were examined by XRD. As shown in Figure 2, it was obvious that only

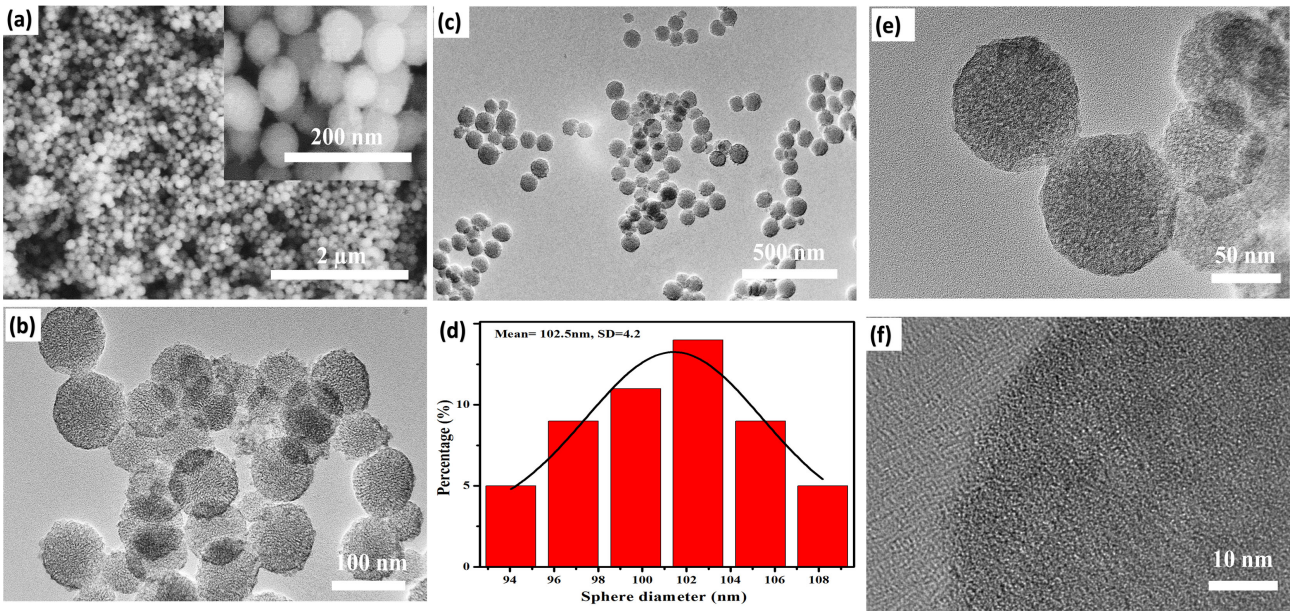

Figure 1. Morphology and structural analysis for the SiO_2:Tb^{3+} spherical nanoparticles: representative low and high-magnification SEM image (a), high-magnification TEM image (b), low-magnification TEM image (c), The diagram histogram of the spherical nanoparticles (d), HR-TEM image (e), SEAD pattern (f).

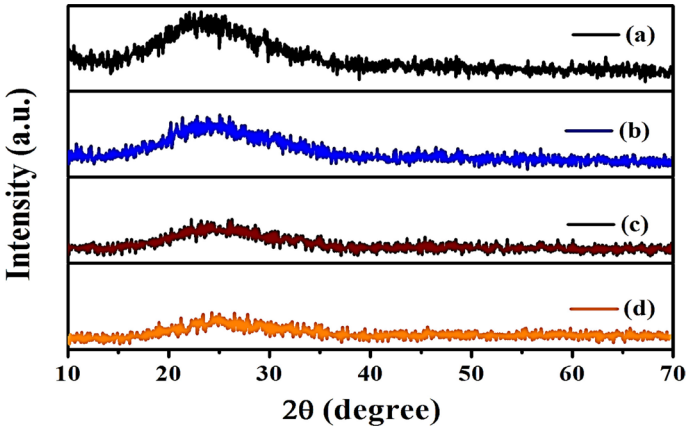

Figure 2. XRD patterns of The SiO_2:xTb^{3+} spherical nanoparticles doping different concentration after calcined at 600˚C (a) x = 0.00; (b) x = 0.02; (c) x = 0.03; (d) x = 0.04.

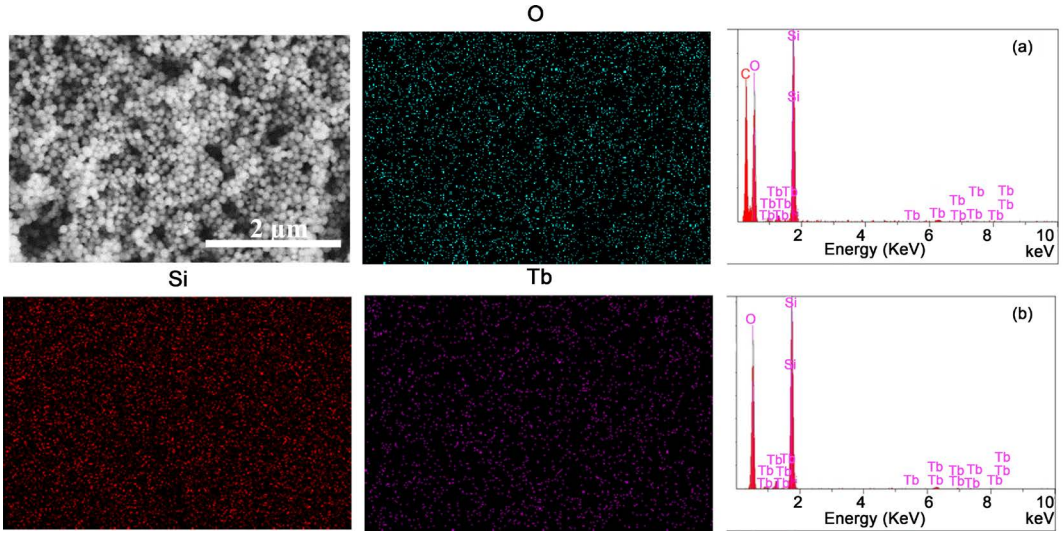

Figure 3. The EDX spectra of SiO_2: 3% Tb^{3+} precursor spheres (a); SiO_2:Tb_{3+} spherical nanoparticles (b) and elemental mapping of SiO_2:Tb^{3+} spherical nanoparticles.

broad peaks could be observed at 2θ = 24˚ - 25˚ in all samples, which corresponding to the characteristic diffraction peak of pure amorphous SiO_2 [22], indicating no other phases or impurities were formed. Meanwhile, it also could be found that the doping could reduce the intensity of samples by increasing concentration. Here, Tb^{3+} ions were hardly substituted with Si^{4+} due to the large difference on the ionic radius between Tb^{3+} and Si^{4+} (The ion radius of Tb^{3+} and Si^{4+} are 1.04 Å and 0.26 Å, respectively) [23]. Thus we speculated that Tb^{3+} ions was incorporated into the network structure of SiO_2 by some weak interaction with O atoms, which reduced the symmetry of SiO_2 framework by deforming the distance of Si-O bond and/or the angle of Si-O-Si bond [24].

3.2. Component Analysis

The EDX spectra for SiO_2:Tb^{3+} precursor spherical nanoparticles and SiO_2:Tb^{3+} spherical nanoparticles were demonstrated to **Figure 3**. That EDX characterization demonstrated that four components carbon (C), silicon (Si), oxygen (O)

and terbium (Tb) were existed in the forerunner spherical nanoparticles, to which those atomic percent of C might have been high. Following calcination during 600˚C, it Might a chance to be seen main three elements, Si, O and Tb were existed in the SiO_2:Tb^{3+} spherical nanoparticles, which intended that C element resulting from organic component (such as CTAB) was completely removed after heat treatment and immaculate SiO_2:Tb^{3+} spherical nanoparticles were acquired. Those element-mapping images depicted those appropriation about Si, O and Tb components for SiO_2:Tb^{3+} spherical nanoparticles by mapping those same district Similarly as the SEM image, which plainly shown that Si, O and Tb atoms were homogeneously disseminated in the SiO_2:Tb^{3+} spherical nanoparticles. All the results above showed that the luminescent Tb^{3+} doped SiO_2 spherical nanoparticles were arranged effectively.

XPS analysis is conducted to get more insight into the chemical composition and electronic structure of the as-prepared SiO_2:Tb^{3+} spheres. **Figure 4** reveals the presence of Si 2p, O 1s, Tb3d, and Tb 4d peaks respectively indicating the formation of SiO_2:Tb^{3+} sphere. The atomic ratio of Si 2P/O 1s/Tb 3d is estimated to be 38.6/61.19/0.77 and 37.6/61.43/0.88 via using 1 and 3 mol % of Tb^{3+}. Intriguingly, the binding energy of Si 2P in SiO_2:Tb^{3+} is blue shifted by 0.12 eV and 0.18 eV upon increasing Tb concentration, similarly the biding energy of O1S is blue shifted by 0.06 eV and 0.12 eV (**Figure 4**). This is ascribed to the doping effect, which alter the electronic structure of Si [25]. Meanwhile, the binding energy of Tb $4d_{3/2}$ is 154.35 and 154.6 eV via using 1 and 3 mol % of Tb^{3+}. The same results were shown in Tb 3d spectra, two new intense peaks around 1277 eV and 1242.9 eV were assigned to the Tb $3d_{5/2}$ and Tb $3d_{3/2}$, respectively (**Figure 4**). These slightly difference arising from change the chemical environment of Tb^{3+} element by doping into the SiO_2 matrix [26].

3.3. Photoluminescence Properties

In **Figure 5** the luminescent properties of the Tb^{3+} doped silica spherical nanoparticles were investigated. The excitation spectra of the Tb^{3+} doped silica spherical nanoparticles after calcination at 600˚C was shown in **Figure 5**, the PL excitation spectra obtained by monitoring a green emission with various concentration of Tb^{3+} at 541 nm revealed a strong absorption ($4f^8$-$4f^75d^1$) and several narrow peaks at 239 nm ($^7F_6$-$^5D_0$), 316 nm (^{7}F6-$^5L_8$), 328 nm ($^7F_6$-^{5}G4), 346 nm ($^7F_6$-$^5G_5$), 358 nm ($^7F_6$-$^5D_3$) and 468 nm ($^7F_6$-$^5D_4$), which were ascribed to the transitions from the 4f to 5d of the Tb^{3+} ions [27]. Under 377 nm UV radiation excitation, the emission spectrum of SiO_2:0.03Tb^{3+} spherical nanoparticles was composed of a group of sharp lines centered at about 487 nm, 541 nm, 583 nm and 618 nm, which corresponding to the $^5D_4$-^7F_J (J = 6, 5, 4 and 3) transitions of the Tb^{3+} ions, respectively, indicating the as-prepared SiO_2:0.03Tb^{3+} spherical nanoparticles exhibit characteristic green emission.

Figure 6 presents the PL emission spectra of the SiO_2:xTb^{3+} samples with different Tb^{3+} concentrations at 377 nm irradiation. We could find that the spectra were almost same irrespective of the Tb^{3+} concentration, but with the increasing

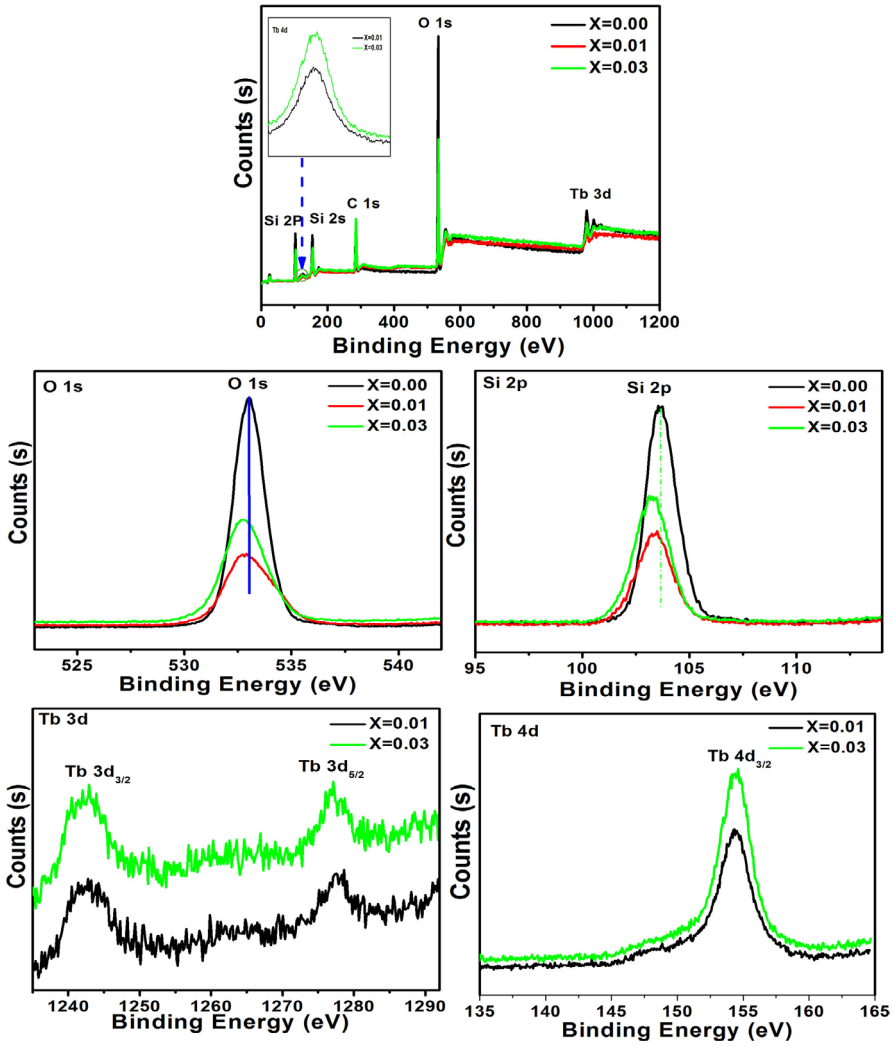

Figure 4. Wide-scan XPS spectra and high-resolution Si (2p), O (1s), Tb (3d) and Tb (4d) XPS spectra of SiO_2:Tb^{3+} spheres.

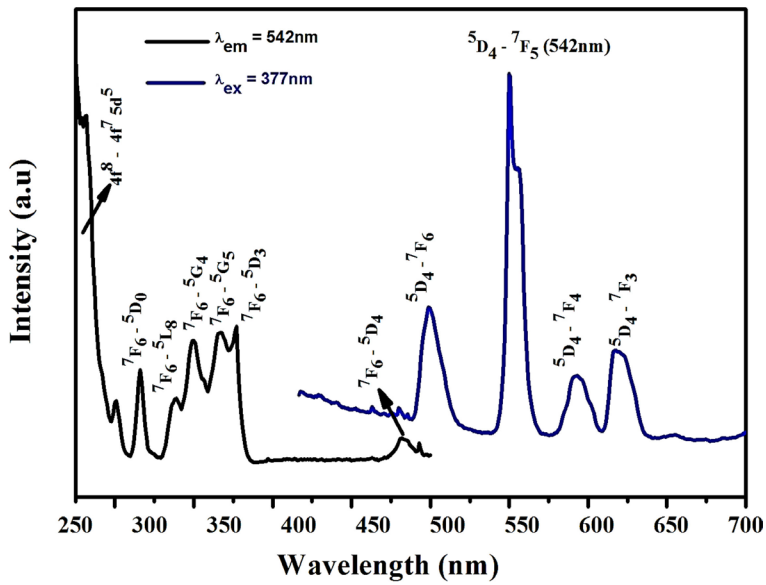

Figure 5. PL excitation and emission spectra of the SiO_2:0.03Tb^{3+} spherical nanoparticles.

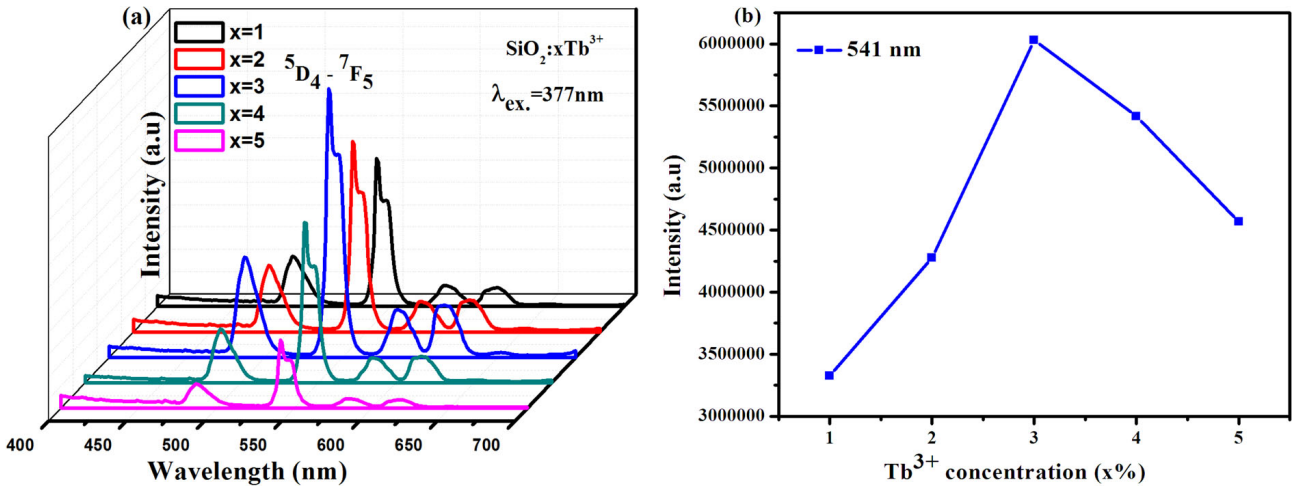

Figure 6. PL emission spectra of SiO2:x%Tb^{3+} spherical nanoparticles with various Tb^{3+} concentrations, (a) T he emission intensity of Tb^{3+} as a function of Tb^{3+} concentration, (b).

of the Tb^{3+} concentration from 1 mol% to 5 mol%, the PL intensity of the $^5D_4 \rightarrow {}^7F_J$ (J = 6, 5, 4, 3) transition increased at first, reaching a maximum value at the concentration of 3 mol%, and then decreased with the increasing of Tb^{3+} content due to the concentration quenching effect [28]. This might be due to the cluster of activators at high concentration would lead to the energy transfer by cross-relaxation between Tb^{3+} ions in the SiO_2:Tb^{3+} sphere. For most of rare-earth activators, the concentration quenching effect was ascribed to the non-radiative energy transfer from rare-earth ions to nearby quenching centers, which usually through the exchange interaction and multipole-multipole interaction [29]. At the same time, other non-radioactive processes such as energy transfer to hydroxyl ions and the defects in silica also could contribute to the luminescence quenching effects. It could be indicated that the optimal doping concentration of Tb^{3+} ions was 3 mol % of spherical nanoparticles. The luminescence property of the Tb^{3+} doped SiO_2 spherical nanoparticles was predominantly attributed to $^5D_4 \rightarrow {}^7F_6$ and $^5D_4 \rightarrow {}^7F_5$, and the $^5D_4 \rightarrow {}^7F_5$ peak was dominant in comparison with other peaks, which was a hypersensitive forced electric dipole transition. It was known that the f-f transition arising from a forced electric dipole was forbidden and became partially allowed when the rare-earth ion was situated at a low symmetry site [23]. Therefore, the Tb^{3+} concentration as well as the silica framework structure affected the efficient luminescence of Tb^{3+} ions [13]. From the results discussed above, it can be deduced that the optimal efficient luminescence was observed at the 3 mol %Tb^{3+}, which means that the concentration quenching was occurred above 3 mol % Tb^{3+}.

The decay kinetics behaviors of Tb^{3+} in SiO_2:xTb^{3+} sphere were investigated. The lifetime decay curves for the $^5D_4$-$^7F_5$ transition of Tb^{3+} (541 nm) at different concentration were measured at room temperature under excitation of 377 nm. As illustrated in **Figure 7**, the decay curves for the $^5D_4$-$^7F_5$ transition of Tb^{3+} in all samples could be fitted well by a double-exponential decay [30]:

$$I(t) = I_0 + A_1 \exp(-t/\tau_1) + A_2 \exp(-t/\tau_2)$$

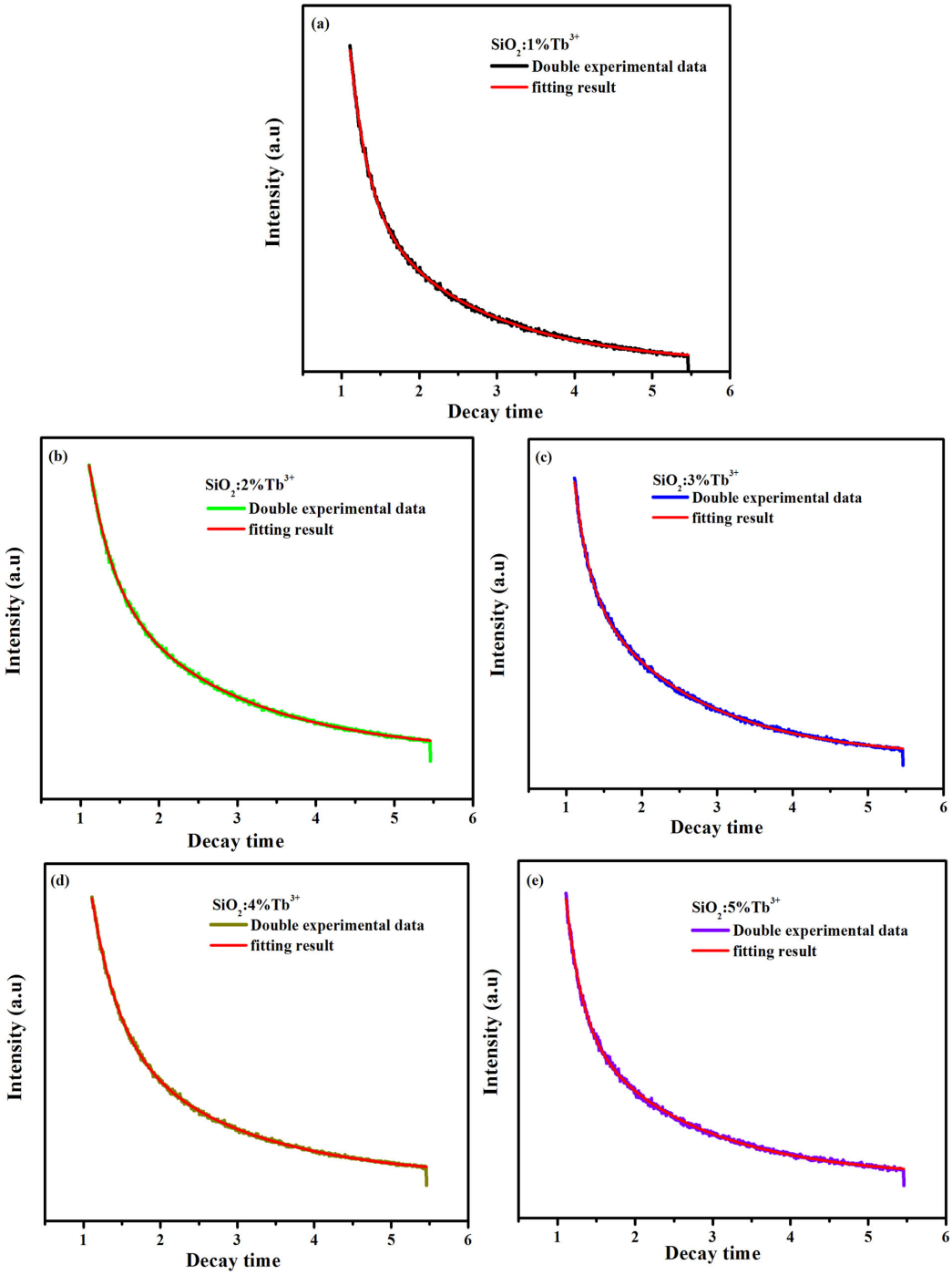

Figure 7. The decay kinetics behaviours of SiO_2:xTb^{3+} spheres for x = 0.01 (a); x = 0.02 (b); x = 0.03 (c); x = 0.04 (d); x = 0.05 (e).

where I and I_0 are the luminescence intensities at time t and 0, A_1 and A_2 are constants, t is the time, and τ_1 and τ_2 are the decay times for the exponential components. Furthermore, the average decay lifetimes (τ) can be calculated as

$$\tau = \left(A_1\tau_1^2 + A_2\tau_2^2\right) / \left(A_1\tau_1 + A_2\tau_2\right)$$

All the curves can be fitted by a double-exponential procedure, and the life-

time values of Tb^{3+} in SiO_2:Tb^{3+} can be determined to be 0.37, 0.74, 1.12, 0.69 and 0.32 ms corresponding to the Tb^{3+} concentration of 1%, 2%, 3%, 4% and 5% respectively. As seen in **Figure 7**, with the increase of the Tb^{3+} content, the lifetime values of SiO_2:xTb^{3+} spheres gradually extended until up to x = 0.03, then tended to decrease. The variation tendency of decay lifetime sequence was consisted with the luminescence intensity of samples. That means both the strongest luminescence intensity and longest lifetime value of Tb^{3+} in SiO_2:xTb^{3+} sphere ware at x = 0.03.

4. Conclusion

In summary, a series of SiO_2:xTb^{3+} spherical nanoparticles with various Tb^{3+} concentrations were successfully prepared via a simple CTAB-based sol-gel process. The as-synthesized samples present a well-defined spherical morphology. Under ultraviolet excitation, the Tb^{3+} singly doped SiO_2 samples show strong green emission. Furthermore, the luminescence intensity of the As-prepared Tb^{3+} doped SiO_2 spherical nanoparticles exhibited a high PL intensity determined by concentration of Tb^{3+} and achieved a maximum PL intensity (6.03027×10^6) at 3 mol% Tb^{3+}. These results indicate that the As-prepared Tb^{3+} doped SiO_2 spherical nanoparticles with variable concentration could be a potential phosphor to be used in the display and solid state lighting fields.

Acknowledgements

This present work was financially supported by the National Natural Science Foundation of China (Grant Nos. 51272085 and 21671078), the Opening Research Funds Projects of the State Key Laboratory of Inorganic Synthesis and Preparative Chemistry and College of Chemistry, Jilin University (2016-06), and Project Supported by Graduate Innovation Fund of Jilin University (2016145). Murad M.A. Abualrejal greatly appreciates Chinese government scholarship 2013.

References

[1] Zhu, G., Ci, Z., Shi, Y., Que, M., Wang, Q. and Wang, Y. (2013) Synthesis, Crystal Structure and Luminescence Characteristics of a Novel Red Phosphor $Ca_{19}Mg_2(PO_4)_{14}$:Eu^{3+} for Light Emitting Diodes and Field Emission Displays. *Journal of Materials Chemistry C*, **1**, 5960-5969. https://doi.org/10.1039/c3tc31263a

[2] Nuñez, N.O., Rivera, S., Alcantara, D., Jesus, M., García-Sevillano, J. and Ocaña, M. (2013) Surface Modified Eu:$GdVO_4$ Nanocrystals for Optical and MRI Imaging. *Dalton Transactions*, **42**, 10725-10734. https://doi.org/10.1039/c3dt50676b

[3] Dai, Y., Ma, P., Cheng, Z., Kang, X., Zhang, X., Hou, Z., Li, C., Yang, D., Zhai, X. and Lin, J. (2012) Up-Conversion Cell Imaging and pH-Induced Thermally Controlled Drug Release from $NaYF_4$:Yb^{3+}/Er^{3+}@ Hydrogel Core-Shell Hybrid Microspheres. *ACS Nano*, **6**, 3327-3338. https://doi.org/10.1021/nn300303q

[4] Gai, S., Li, C., Yang, P. and Lin, J. (2013) Recent Progress in Rare Earth Micro/Nanocrystals: Soft Chemical Synthesis, Luminescent Properties, and Biomedical Applications. *Chemical Reviews*, **114**, 2343-2389. https://doi.org/10.1021/cr4001594

[5] Raju, G.S.R., Pavitra, E., Nagaraju, G.P., Ramesh, K., El-Rayes, B.F. and Yu, J.S. (2014) Imaging and Curcumin Delivery in Pancreatic Cancer Cell Lines Using PEGylated α-$Gd_2(MoO_4)_3$ Mesoporous Particles. *Dalton Transactions*, **43**, 3330-3338. https://doi.org/10.1039/C3DT52692E

[6] Seeta Rama Raju, G., Pavitra, E., Nagaraju, G.P., Kandimalla, R., El-Rayes, B.F. and Yu, J.S. (2013) PEGylated α-$Gd_2(MoO_4)_3$ Mesoporous Flowers: Synthesis, Characterization, and Biological Application. *Crystal Growth & Design*, **13**, 4051-4058. https://doi.org/10.1021/cg400893h

[7] Birkel, A., Denault, K.A., George, N.C., Doll, C.E., Hery, B., Mikhailovsky, A.A., Birkel, C.S., Hong, B.-C. and Seshadri, R. (2012) Rapid Microwave Preparation of Highly Efficient Ce^{3+}-Substituted Garnet Phosphors for Solid State White Lighting. *Chemistry of Materials*, **24**, 1198-1204. https://doi.org/10.1021/cm3000238

[8] Wu, W. and Xia, Z. (2013) Synthesis and Color-Tunable Luminescence Properties of Eu^{2+} and Mn^{2+}-Activated $Ca_3Mg_3(PO_4)_4$ Phosphor for Solid State Lighting. *RSC Advances*, **3**, 6051-6057. https://doi.org/10.1039/c3ra40313k

[9] Rao, G.M., Hussain, S.K., Raju, G.S.R., Rao, P.S. and Yu, J.S. (2016) Synthesis and Characterizations of Novel $Sr_2Gd_8(SiO_4)6O_2$:Eu^{3+} Oxyapatite Phosphors for Solid-State Lighting and Display Applications. *Journal of Alloys and Compounds*, **660**, 437-445.

[10] Armelao, L., Belli Dell'Amico, D., Bellucci, L., Bottaro, G., Labella, L., Marchetti, F. and Samaritani, S. (2016) Smart Grafting of Lanthanides onto Silica via *N*,*N*-Dialkylcarbamato Complexes. *Inorganic Chemistry*, **55**, 939-947. https://doi.org/10.1021/acs.inorgchem.5b02535

[11] Li, W. and Zhao, D. (2013) Extension of the Stöber Method to Construct Mesoporous SiO_2 and TiO_2 Shells for Uniform Multifunctional Core-Shell Structures. *Advanced Materials*, **25**, 142-149. https://doi.org/10.1002/adma.201203547

[12] Pradhan, N., Rhodes, D., Zhang, Q., Talapatra, S., Terrones, M., Ajayan, P. and Balicas, L. (2013) Intrinsic Carrier Mobility of Multi-Layered MoS_2 Field-Effect Transistors on SiO_2. *Applied Physics Letters*, **102**, Article ID: 123105. https://doi.org/10.1063/1.4799172

[13] Bai, Z., Chen, R., Si, P., Huang, Y., Sun, H. and Kim, D.-H. (2013) Fluorescent pH Sensor Based on Ag@SiO_2 Core-Shell Nanoparticle. ACS *Applied Materials & Interfaces*, **5**, 5856-5860. https://doi.org/10.1021/am401528w

[14] Yan, N., Wang, F., Zhong, H., Li, Y., Wang, Y., Hu, L. and Chen, Q. (2013) Hollow Porous SiO_2 Nanocubes towards High-Performance Anodes for Lithium-Ion Batteries. *Scientific Reports*, **3**, Article No. 1568. https://doi.org/10.1038/srep01568

[15] Wong, Y.J., Zhu, L., Teo, W.S., Tan, Y.W., Yang, Y., Wang, C. and Chen, H. (2011) Revisiting the Stober Method: Inhomogeneity in Silica Shells. *Journal of the American Chemical Society*, **133**, 11422-11425. https://doi.org/10.1021/ja203316q

[16] Makhinson, B., Duncan, A.K., Elam, A.R., de Bettencourt-Dias, A., Medley, C.D., Smith, J.E. and Werner, E.J. (2013) Turning on Lanthanide Luminescence via Nanoencapsulation. *Inorganic Chemistry*, **52**, 6311-6318. https://doi.org/10.1021/ic3022722

[17] Liu, X.-L., Zhu, P.-X., Gao, Y.-F. and Jin, R.-H. (2013) Synthesis of Free-Standing sub-10 nm Y_2O_3:Eu Particles on Silica Nanowire Matrix and Amplified Luminescence Performance. *Journal of Materials Chemistry C*, **1**, 477-483.

[18] Qiao, Y., Chen, H., Lin, Y., Yang, Z., Cheng, X. and Huang, J. (2011) Photoluminescent Lanthanide-Doped Silica Nanotubes: Sol-Gel Transcription from Functional Template. *The Journal of Physical Chemistry C*, **115**, 7323-7330. https://doi.org/10.1021/jp200515s

[19] Chen, J., Sheng, Y., Zhou, X., Abualrejal, M.M., Chang, M., Shi, Z. and Zou, H. (2016) Dendrimer-Based Preparation and Luminescence Studies of SiO_2 Fibers Doping Eu^{3+} Activator in Interstitial Sites. *RSC Advances*, **6**, 16452-16460. https://doi.org/10.1039/C5RA25859F

[20] Gao, F., Sheng, Y., Song, Y., Zheng, K., Lin, C., Zhang, H., Huo, Q. and Zou, H. (2014) Facile Synthesis and Luminescence Properties of Europium (III)-Doped Silica Nanotubes. *Journal of Sol-Gel Science and Technology*, **71**, 313-323. https://doi.org/10.1007/s10971-014-3368-7

[21] Choi, Y.I., Yoon, Y., Kang, J.-G. and Sohn, Y. (2015) Photoluminescence Imaging of Eu(III) and Tb(III)-Embedded SiO_2 Nanostructures. *Journal of Luminescence*, **158**, 27-31.

[22] Zulkifli, N.S.C., Ab Rahman, I., Mohamad, D. and Husein, A. (2013) A Green Sol-Gel Route for the Synthesis of Structurally Controlled Silica Particles from Rice Husk for Dental Composite Filler. *Ceramics International*, **39**, 4559-4567.

[23] Li, K., Zhang, Y., Li, X., Shang, M., Lian, H. and Lin, J. (2015) Host-Sensitized Luminescence in $LaNbO_4$:Ln^{3+}(Ln^{3+} = Eu^{3+}/Tb^{3+}/Dy^{3+}) with Different Emission Colors. *Physical Chemistry Chemical Physics*, **17**, 4283-4292. https://doi.org/10.1039/C4CP03894K

[24] Tagaya, M., Ikoma, T., Yoshioka, T., Motozuka, S., Xu, Z., Minami, F. and Tanaka, J. (2011) Synthesis and Luminescence Properties of Eu(III)-Doped Nanoporous Silica Spheres. *Journal of Colloid and Interface Science*, **363**, 456-464.

[25] Kim, D., Jin, Y.-H., Jeon, K.-W., Kim, S., Kim, S.-J., Han, O.H., Seo, D.-K. and Park, J.-C. (2015) Blue-Silica by Eu^{2+}-Activator Occupied in Interstitial Sites. *RSC Advances*, **5**, 74790-74801. https://doi.org/10.1039/C5RA15641F

[26] Yan, M., Zou, H., Zhao, H., Song, Y., Zheng, K., Sheng, Y., Wang, G. and Huo, Q. (2014) Fabrication and Photoluminescence Properties of TiO_2:Eu^{3+} Microspheres with Tunable Structure from Solid to Core-Shell. *CrystEngComm*, **16**, 9216-9223. https://doi.org/10.1039/C4CE01048E

[27] Reddy, G.L., Moorthy, L.R., Chengaiah, T. and Jamalaiah, B. (2014) Multi-Color Emission Tunability and Energy Transfer Studies of $YAl_3(BO_3)_4$:Eu^{3+}/Tb^{3+} Phosphors. *Ceramics International*, **40**, 3399-3410.

[28] Koao, L., Swart, H., Obed, R. and Dejene, F. (2011) Synthesis and Characterization of Ce^{3+} Doped Silica (SiO_2) Nanoparticles. *Journal of Luminescence*, **131**, 249-1254.

[29] Du, P., Song, L., Xiong, J., Cao, H., Xi, Z., Guo, S., Wang, N. and Chen, J. (2012) Electrospinning Fabrication and Luminescent Properties of $SrMoO_4$:Sm^{3+} Nanofibers. *Journal of Alloys and Compounds*, **540**, 179-183.

[30] Wang, L.-L., Wang, Q.-L., Xu, X.-Y., Li, J.-Z., Gao, L.-B., Kang, W.-K., Shi, J.-S. and Wang, J. (2013) Energy Transfer from Bi^{3+} to Eu^{3+} Triggers Exceptional Long-Wavelength Excitation Band in $ZnWO_4$:Bi^{3+}, Eu^{3+} Phosphors. *Journal of Materials Chemistry C*, **1**, 8033-8040. https://doi.org/10.1039/c3tc31160k